Synthesis and characterization of the conductivity and Polarization processes in Supported Ionic Liquid-Like Phases (SILLPs)

Vicente Compañ[a,*], Sergio Molla[a], Eduardo García-Verdugo[b], Santiago V. Luis[b], M. Isabel Burguete[b],

[a] *Dpto. de Termodinámica Aplicada, Universidad Politécnica de Valencia, C/Camino de Vera s/n, 46020, Valencia (Spain), Phone. 34-963879328, Fax: 34-963877329, E-mail: vicommo@ter.upv.es*
[b] *Dpto. Química Inorgánica y Orgánica, Universidad Jaume I, Avda. Sos, Baynat s/n, 12071, Castellon, Spain. Fax: +34964728214; Tel: +34 964728239.*

** To whom correspondence will be addressed: Vicente Compañ. E-mail: vicommo@ter.upv.es.*

Keywords: Supported Ionic liquids, SILLPs, ionic conductivity, polarization.

Abstract

Different crosslinked polystyrene resins containing ionic liquid fragments covalently attached (Supported Ionic Liquid-Like Phases: SILLPs) have been prepared and their conductivity has been studied by means of dielectric impedance spectroscopy. The main structural parameters considered in this study have been the presence of C2-H bonds in the imidazolium subunits and the nature (level of hydrophobicity) of the N-substituents (methyl vs. butyl). The results obtained have allowed shows that the presence of C2-H fragments can have an influence on intrinsic conductivity. In the same way the role of the hydrophobicity of the N-substituents seems to play only a minor role. The main structural component associated to conductivity is the nature of the counteranion. The bulkiest, less coordinating anions, in particular the NTf_2^- anion, seem to be associated to the highest conductivities, being the values obtained two orders of magnitude higher than those calculated for the same systems containing the Cl^- anions for each of the temperatures under study. The results obtained rule out the participation of some given conduction mechanisms such as the involvement of carbene formation. Instead, the formation of ion-pairs of higher or lower association (strong/weak ion pairs) can be the responsible of the observed behaviour.

1. Introduction

Ionic liquids (IL) represent an area of research of growing interest nowadays [1]. Many different applications, in particular in the area of Green Chemistry have been reported, in the last years, involving the use of ILs [2]. The essentially non-vapor pressure of ILs has allowed for their use as green solvents as substitutes of many traditional organic solvents characterized for being a source for volatile organic compounds (VOCs). Nevertheless, the use of ILs in Chemistry is going far beyond their use as substitutes for those VOCs generating solvents. Their unique physico-chemical properties have led to the development of new applications and processes that had not been achieved before [3]. Some of those key applications can be found, for instance, in the field of solubilisation of natural macromolecules (carbohydrates, proteins, polynucleotides…) and in the field of catalysis [4]. On the other hand, pioneering work in this field was developed with the essential goal of developing novel electrolytes for different electrochemical applications and thus ILs have become an important component for many electrochemical processes [5], as is the case, for instance, for the development of new generations of photovoltaic devices [6].

Nevertheless, in spite of this blooming of applications for ILs, there are still some drawbacks that are associated to their use as bulk liquids or solvents. First of all, most ILs, in particular those involved in specific applications (task specific ILs: TSILs) [7], continue being rather expensive and their technological application requires developing the proper methodologies for their recovery and reuse. In second place, recent toxicological studies have revealed that although they do not contribute to the generation of VOCs they can have some toxicological or ecotoxicological effects so that an increasing environmental concern is building up on the use of some of those “green solvents” [8]. One simple way to overcome those limitations is the use of supported ionic liquids [9]. Two main approaches can be considered for this purpose. The first one is the adsorption of a small layer of the IL on the surface of an appropriate material (i.e. silica). The so-called Supported-Ionic-Liquid Phases (SILPs) can thus be easily handled and separated for their reuse from the liquid or gas phase being in contact with them for the corresponding process. Although very useful, this approach does not guarantee, in some cases, the total absence of leaching of IL to the reaction media or, finally, to the environment. The second approach is the covalent attachment of IL-like moieties to a

solid support to provide surfaces having macro and microscopic properties very much alike to those of the bulk ILs. The so-called Supported Ionic Liquid-Like Phases (SILLPs), provided an efficient transfer of the IL properties to the solid phase, allow obviating the problem of leaching and guaranteeing, at a higher extent, the recovery and recycling of the system. In this field, the preparation of lineal polymers containing IL-like fragments such as imidazolium, pyridinium, ammonium or phosphonium has been considered for the preparation of solid electrolytes for different applications [10]. Recently we have shown that, in spite of the lower flexibility and mobility of the corresponding polymeric chains, highly crosslinked polystyrene-divinylbenzene polymers functionalized with imidazolium subunits can also provide a response to electrical perturbation fields, as studied by impedance spectroscopy [11].

Central to the wide application of ionic liquids in different fields is their modular character, which is exemplified in chart 1 for the structure of imidazolium ILs.

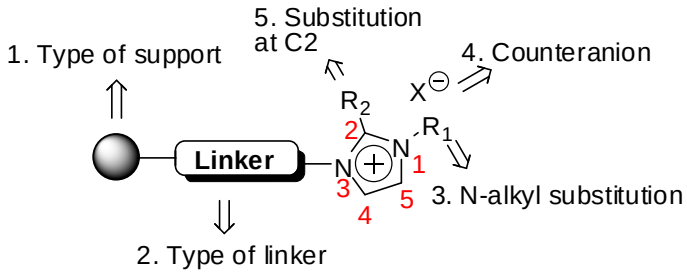

Chart 1. Design vectors for the synthesis of imidazolium base SILLPs.

Changes in the nature of the different substituents in the cationic fragment as well as modifications in the structure of the counteranion provide an essentially infinite series of ILs with modulated properties. This has lead to define those systems as design solvents, as it can be considered that we can always design the optimum IL for a given specific application. We have recently demonstrated that similar variations in the case of supported ionic liquids can be used to tune characteristic of the SILLPs leading to advanced materials with adjustable chemical and physical properties [12]. Taking this into consideration, we have approached here the study of how structural variations in the structure of the IL fragments can affect to their response to an electrical perturbation field. In this regard, two main parameters have been considered: i) the substitution of a N-methyl substituent in the cation for a more hydrophobic N-butyl substituent; ii) the substitution of the C2-H bond by a C2-methyl bond (see chart 1 for the proper

numbering of the imidazolium ring). This last modification is considered in order to understand the importance of the potential hydrogen bonds between the hydrogen at C2 and the counteranion in the conductive processes. Besides, the substitution of the chloride anion by the NTf_2^- anion has been considered, a structural factor that had been studied previously [11].

2. Experimental Part

2.1. Materials

Chloromethylstyrene (Aldrich), divinyl benzene (Aldrich), 1-methylimidazole (Aldrich), lithium bis(trifluormethanesulfonyl)amide ($LiNTf_2$) (Aldrich), MeOH, toluene and dodecanol were used as received. The preparation of the monolithic polymeric rods from chloromethylstyrene and divinyl benzene was carried out as described elsewhere [13].

2.2. Synthesis of monolithic Supported Ionic Liquid-Like Phases (SILLPs)

The synthesis of the corresponding SILLPs was carried out as outlined in the Figure 1, following the standard methodology previously developed by the group of of Castellón [13]. Rods of the support material were prepared by copolymerization of 1-(chloromethyl)-4-vinylbenzene (ClVB) and divinyl benzene (DVB) in a glass mould, under nitrogen atmosphere. The polymerization reaction was carried out for 24 h at 70ºC, using 1% AIBN as initiator. The initial reactants composition of was 40:60 wt%, (ClVB/ DVB) and the reaction medium was a mixture of toluene/dodecanol, 10:50 wt % [13]. Reaction of the chloromethyl groups in the resulting polymer with the corresponding N-alkyl imidazole afforded the corresponding supported imidazolium chlorides, while anion exchange provided the respective bistrifluoroamides (Figure 1). Thus, four SILLPs differing in the structure of the cation and in the nature of the counterion, with acronyms **KN7, KN8**, **KN9** and **KN10** were prepared. Related SILLPs, derived from methyl imidazole (R_1 = CH_3, R_2 = H) had been previously prepared and studied [11].

The **KN7** sample was obtained by introducing the crosslinked ClVB/DVB rod (0.5g, 60% cross-linking, 3.07 mmol Cl/g, 1.53 mmol) into a round-bottomed flask containing 1-butylimidazole (5 mL, 38.04 mmol). The suspension was heated at 80 ºC for 1 h.

Then, the reaction was filtered and the polymer was washed with MeOH, MeOH:CH_2Cl_2 (1:1) and CH_2Cl_2 and dried in a vacuum oven.

FT-IR(cm^{-1}) KBr: 1603; 1509; 1447; 1157; 903; 829; 709. Raman (cm^{-1}): 1599; 1434; 1405; 1301; 1172; 989; 819. Elemental analysis calculated for $(C_{10}H_{10})_{64}$ $(C_{16}H_{21}ClN_2)_{36}$: %N 5.51; %C 72.67; %H 6.45.; found: %N 5.48.

The **KN8** sample was obtained by introducing the crosslinked ClVB/DVB rod (0.5 g, 60% cross-linking, 3.07 mmol Cl/g, 1.53 mmol) into a round-bottomed flask and suspended in a solution 1M of 1,2-dimethylimidazole (5 mL, 56.38 mmol) in DMF. The suspension was heated at 80 ºC for 12 hours. Then the reaction was filtered and the polymer was washed with MeOH, MeOH:CH_2Cl_2 (1:1) and CH_2Cl_2 and dried in a vacuum oven.

IR(cm^{-1}) KBr: 1602, 1587, 1535, 1512, 1451, 1421, 1269, 1239, 1162, 1112, 1081, 1019, 855, 762, 665, 607, 545 Raman (cm^{-1}): 1595, 1575, 1506, 1442, 1323, 1192, 1177, 1148, 1064, 1024, 995, 900, 825, 755, 720, 663, 637, 616, 540, 401, 310. Elemental analysis calculated for $(C_{10}H_{10})_{0.64}$ $(C_{14}H_{17}ClN_2)_{0.36}$: %N 5.83; %C 82.33; %H 7.24.; found: %N 4.68.

KN9. The monolithic rod **KN7** (0.5g, 0.98 mmol) was suspended in 5 mL of MeOH. $LiNTf_2$ (3 eq.) was dissolved in 0.5 mL of miliQ water and added to the suspension. The system was stirred for 24 h at r.t. Then, the polymer was filtered and washed (3x20 mL) with MeOH, MeOH:water (1:1), MeOH and CH_2Cl_2. Finally, the polymer was vacuum dried.

FT-IR(cm^{-1}) KBr: 1558, 1348, 1183, 1133, 1054, 790, 739, 708, 614. Raman (cm^{-1}): 1620, 1601, 1400, 1308, 1175, 992, 821, 735, 636. Elemental analysis calculated for $(C_{10}H_{10})_{64}$ $(C_{18}H_{21}F_6O_4\ S_2N_3)_{36}$: %N 5.58; %C 57.05; %H 5.15; %S 8.50.; found: %N 3.57

KN10. The monolithic rod **KN8** (0.5g, 1.04mmol) was suspended in 5 mL of MeOH. $LiNTf_2$ (3 eq.) was dissolved in 0.5 mL of miliQ water and added to the suspension. The system was stirred for 24 h at r.t. Then, the polymer was filtered and washed (3x20 mL) with MeOH, MeOH:water (1:1), MeOH and CH_2Cl_2. Finally, the polymer was vacuum dried.

FT-IR(cm^{-1}) KBr: 1572, 1353, 1195, 1057, 618, 513. Raman (cm^{-1}): 1606, 1408, 1380, 1324, 1234, 1181, 1085, 1015, 995, 965, 826, 735, 636, 614 Elemental analysis calculated for $(C_{10}H_{10})_{0.64}$ $(C_{16}H_{17}F_6N_3O_4S_2)_{0.36}$: %N 5.80; %C 55.95; %H 4.80; %S 8.83.; found: %N 5.48.

2.3. Differential scanning calorimetry

DSC curves were obtained using a Metler Toledo 831-DSC device at 10 K/min rate under nitrogen atmosphere. The thermograms shown in Figure 2 present weak endotherms apparently associated with the glass transition temperature of these crosslinked systems. The departure of the endotherms from the base line in the low temperature side, was taken as the glass transition temperature. The values of this temperature for **KN7**, **KN8**, **KN9** and **KN10** were found to be approximately 35, 51, 45 and 62 ºC, respectively (see magnification of Figure 2). The presence of those clearly observable peaks suggests the presence of an ordered structure for the IL-like fragments on the surface of the polymer that is disordered upon heating. It is worth nothing that for the SILLPs containing Cl^- as the anion (**KN7** and **KN8**) the system having a methyl group at the C-2 position of the imidazolium ring presents a lower transition temperature. A similar effect, but at a lower extent is observed for the systems containing the NTf_2^- anion (**KN9** and **KN10**). This suggests that intermolecular hydrogen bond formation can be an important factor to establish the abovementioned ordered structure, besides coulombic interactions. This is in good agreement with the observations made for related polymers **KN5** ($R_1 = CH_3$, $R_2 = H$, Cl^- anion) and **KN6** ($R_1 = CH_3$, $R_2 = H$, NTf_2^- anion) [11].

2.4. Impedance and dielectric measurements

Impedance experiments were carried out on SILLPs samples at several temperatures lying in the range 298 K (25ºC) to 398 K (125ºC) and frequency window $10^{-2} < f < 10^6$ Hz. The measurements were performed with 100 mV amplitude, using a Novocontrol

broadband dielectric spectrometer (Hundsangen, Germany) integrated by a SR 830 lock-in amplifier with an Alpha dielectric interface. The SILLP sample of interest was placed between two gold electrodes coupled to the impedance spectrometer. The temperature was controlled by a nitrogen jet (QUATRO from Novocontrol) with a temperature error of 0.1 K during every single sweep in frequency.

3. Results

The impedance response is usually measured with blocking electrode/polar system/blocking electrode configuration. Figures 3 and 4 shows Bode diagrams [14-15] for the complex impedance module and phase corresponding to the dielectric spectra of the SILLPs KN7 and KN9 in the temperature range 298 K to 398 K, respectively. At high temperatures, the isotherms are characterized by a plateau nearly independent on frequency, followed by a dispersive regime. Moreover, whereas the plateau for the **KN9** isotherms coexists with $\phi = 0$ in a wide range of temperatures, this only occurs for the **KN7** system at high temperatures. For low temperatures the values of $/\phi/$ at the frequencies studied are higher than zero, indicating that in these cases the ohmic resistance should be slightly higher than the maximum value of $/Z^*(\omega)/$ at the apparent plateau. Thus, obtaining the whole Bode diagram would surely require measuring the impedance at frequencies significantly lower than those used in this study. For frequencies where the phase is near zero we have pure resistive impedance that can be attributed to the ionic conductivity alone. For phases near -90º, besides resistive impedance we have capacitance effects that correspond to the charge accumulation due to the macroscopic Debye polarization. Then R_o is taken as the magnitude of the impedance ($/Z^*(\omega)/$) at the plateau coexisting with $\phi = 0$. Similar behavior as observed in Figure 3 has been obtained for **KN8,** and for **KN10** the response was very similar to that observed in Figure 4 for **KN9**. From Figures 3 and 4 we can see that the length of the plateau in the Bode diagrams increases as temperature increases until a critical frequency f_c ($= \omega_c/2\pi$), dependent on temperature, is reached, at which $\log /Z^*(\omega/$ collapses along a straight line with slope $d \log /Z^*(\omega/ / d \log \omega = -1$. This is a typical behavior of a parallel R_0C circuit, where at high frequencies at which $\omega C >> 1$ and

$$\lim_{\omega\to\infty} \log\left|Z^*(\omega)\right| = \lim_{\omega\to\infty} \log\left|\frac{R_o}{1+ j\omega R_o C}\right| \cong \log\left(\frac{1}{C\omega}\right) \quad (1)$$

And for low frequencies at which $\omega C << 1$, then $\lim_{\omega \to 0} |Z^*(\omega)| = R_0$.

Thus for frequencies $\omega \leq 1/(R_0 C)$, the magnitude of the impedance is practically constant, for each temperature, and the dc-conductivity can be determined from the pleateau observed in the Bode diagrams. However above the critical frequency $\omega_c \geq 1/(RoC)$, the impedance is eminently capacitive and $|Z^*(\omega)| \propto \omega^{-1}$, in agreement with the results shown in the Bode diagrams of Figures 3a and 4a. The critical frequency was taken as that one corresponding to the inflexion point of the phase angle, i.e. $\phi = -45^o$, at the temperature of interest. The conductivities of the SILLPs were calculated from the resistances obtained from the Bode diagrams by means of the expression

$$\sigma = \frac{l}{R_o S} \qquad (2)$$

where σ, S and l are, respectively, the ohmic conductivity, area and thickness of the rod in contact with the blocking electrodes. The values of the conductivity obtained for **KN7**, **KN8**, **KN9** and **KN10** from Bode diagrams for each temperature studied are collected in Table 1.

The activation plot of Figure 5 shows the dependence of the critical frequency ω_c ($\omega_c = 2\pi f_c$) with the temperature. Apparently, there seems to be an Arrhenius behavior, but this may be due because the data are analyzed for a narrow temperature range and in such cases any temperature dependence present Arrhenius behavior. According to this, in Figure 5 for example, when the data cover broader range (e.g. 4 orders or decades for **KN9** and **KN10**, it is clear that this pseudo-Arrhenius behavior is only apparent. For this the calculated activation energies associated to the process are only apparent values. The results found are (16.2±0.3), (20.5±1.0.3), (26.2±0.7) and (25.7±0.6) kcal mol^{-1} for **KN7**, **KN8**, **KN9** and **KN10**, respectively. The precision of the activation energy coefficient, was estimated from the slope (m) of the Arrhenius plot for dc-conductivity and the correlation coefficient of the straight line r, according to the expression

$$\varepsilon(m) = m \frac{\tan(\arccos(r))}{\sqrt{N-2}} \qquad (3)$$

Where N is the number of experimental points used for the straight line determination.

Moreover, the capacity of the geometric capacitors are independent on temperature their values being (1.07±0.04), (1.55±0.05), (2.30±0.12), and (2.56±0.12)

pF for **KN7**, **KN8**, **KN9** and **KN10**, respectively. The precision have seen estimated from the plotting the eq(1) in the range of frequencies where the impedance is eminently capacitive. From slope and the correlation coefficient using the eq.(3) the errors have seen obtained. From these results we can conclude that the charge accumulation due to the macroscopic Debye polarization follow in the SILLPs studied de following trends KN10>KN9>KN8>KN7.

The impedance patterns showed in the Bode diagrams of Figures 3 and 4 show exhibit a frequency independent plateau in the low frequency region and exhibit dispersion at higher frequencies. This behavior obeys the power law [16], $\left|\sigma^*(\omega)\right| = \sigma_0 + A \cdot \omega^n$, where σ_0 is the dc-conductivity (frequency independent plateau in the low frequency region), A is the pre-exponencial factor and *n* is the fractional exponent between 0 and 1. The effect of the electrode polarization is evidenced in a small deviation from the σ_{dc} (plateau region) value in the conductivity spectrum. This is even more clearly observed in the diagrams on the right side of Figures 3 and 4 displaying the real part of the conductivity *versus* frequency. The ionic conductivity thus estimated for **KN7** and **KN8** is rather low, increasing in the former material from 4.9×10^{-12} S/cm, at 328 K (55º C), to ca. 1.4×10^{-9} S/cm, at 398 K (125º C), S/cm, whereas in the SILLP **KN8** the increase is from 1.1×10^{-11} S/cm, at 328 K (55º C), to ca. 2.1×10^{-9} S/cm, at 398 K (125º C), S/cm. Whereas the comparison of the ionic conductivity between **KN9** and **KN10** is estimated to change from 4.7×10^{-11} to 5.3×10^{-7} S/cm and 3.1×10^{-12} at 303 K (35ºC) to 2.3×10^{-7} S/cm at 398 K (125º C), in the same range of temperature. As shown in Figure 6, the temperature dependence of the conductivity is also a thermally activated process described by a pseudo-Arrhenius behavior this may be due because the data are analyzed for a narrow temperature range. The apparent activation energies obtained from this plot are given in table 1. The precision of the activation energy coefficient was estimated from the slope of the pseudo-Arrhenius plot for dc-conductivity and the correlation coefficient of the straight line.

Illustrative experimental isotherms showing the components of the complex dielectric permittivity in the frequency domain for **KN10** are presented at several temperatures in Figure 7. For temperatures lower than 338 K (65 ºC), ε' is only slightly dependent on frequency in the range $0.01 \leq f \leq 10^6$ Hz. Identical behavior has been observed for the others SILLPs **KN7**, **KN8** and **KN9**. At higher temperatures, ε'

undergoes a significant increase as frequency decreases, the increase being higher with temperatures. This augment of ε' is the result of the enhancement on the mobility of the chains occurring when the systems surpass the glass transition temperature. However, the plateau exhibited by the real component of ε* at low frequencies in polar polymers [14,17] is not reached in the SILLPs in the range of temperatures studied.

As for the dielectric loss, the isotherms present a dielectric dispersion in the high frequency region of the spectra, only detectable in the isotherms obtained at high temperature. At moderate and low frequencies ε'' is nearly a linear increasing function of the reciprocal of the frequency and as a result dielectric dispersions associated with the dielectric loss are obscured by the conductivity.

When discussing the results presented in Figure 7, we have noted that the dielectric permittivity ε" is high increasing with temperature in the low frequency region, and shows a straight line at low frequencies with slope compress in the range 0.9 to 1, which we attributed to a conduction process, although an important participation of electrode polarization can also be involved. In order to explore this phenomenon in detail, we used the electric modulus formalism M* to rendering [18,19].

Despite some doubts cast on the applicability of the method for this task [20,21], a combined study of ionic motion using electrical relaxation and Nuclear Magnetic Resonance (NMR) relaxations suggests that the complex modulus is an appropriate representation of dielectric data for analysis of ionic conductivity relaxation as in the present case. The points made by Elliot and Roling in Refs. 20 and 21 as well by others to discredit the dielectric modulus representation have been refuted and are summarily discussed in a review article [22] where the authors have answered all the unnecessary criticism on the use of the electric modulus. The representation of the macroscopic data to describe the microscopic motion of the movement of the ions has been also well described, as in the present case, in Ref. 23.

The electric modulus is the reciprocal of the permittivity $M^*=1/\varepsilon^*$, where $M^*=M'+iM''$; M' and M'' are the real and imaginary parts, respectively. Generally, for a pure conduction process, a relaxation peak would be observed in the frequency spectra of the imaginary component M'' and no peak would take place in the corresponding plot of ε'', as is our case. The equivalence of the frequency of the peak in the imaginary part of the complex modulus M", and the characteristic frequency f_c at which the real part of

the conductivity (σ') begins to increase with increasing frequency for disordered ion conducting solids has been pointed out by a number of researchers [24-29].

In Figure 5, these two rates are compared for **KN7**, **KN8**, **KN9** and **KN10**. The remarkable coincidence obtained indicates that f_c and f_M in ionic liquids describe an identical underlying activation process; that is, electrical relaxation or more properly the conductivity associated to the α-relaxation of the polymer. The apparent activation energies obtained from the characteristic electrical rates, f_M, are (20,4±0,4), (18,9±0,7), (25,1±0,5), and (28,5±0,5), kcal/mol for **KN7, KN8, KN9** and **KN10**, respectively. A comparison between these values and the ones obtained from the conductivity calculated from the Bode diagrams are in complete agreement, indicating that ionic transport in the SILLPs is at their origin.

Isotherms at several temperatures showing the double logarithmic plots of the real and imaginary components of the complex dielectric modulus of **KN7**, **KN8**, **KN9** and **KN10** are shown in the frequency domain in Figures 8, 9, 10 and 11, respectively. As occurs with the modulus of relaxation processes, *M'* increases as the frequency increases until a frequency is reached at which *M'* remains nearly constant. Moreover, *M''* displays at low frequencies the characteristic absorption of conductive processes and a *M"* peak in the plots of *M" vs.* frequency is observed in relation to the conductivity relaxation of the SILLPs. In addition to the conduction peak, a second peak can be seen in some cases at high temperatures, which shifts to higher frequency with a very small absorption, such as happened on SILLPs **KN5** and **KN6** [11]. In this case, these peaks indicate the transition from short range to long range mobility with decreasing frequency, where the low frequency side of the peak represents moving long distances, i.e., performing successful hopping from one site to the neighboring site, whereas, for the high frequency side, the ions are spatially confined to their potential wells and can execute only localized motion [30,31].

In the low frequency region, *M'* and *M''* follow the predictions of the linear theory of dielectrics for relaxation moduli in such a way that $\lim_{\omega\to 0}\left[d\,M'(\omega)/d\log\omega\right]=2$ and $\lim_{\omega\to 0}\left[d\,M''(\omega)/d\log\omega\right]=1$.

The relaxation of the dielectric modulus can be mathematically represented equivalently as a function of time or of frequency. This approach developed for a single relaxation time for dielectric relaxations by Debye has been extended by Havriliak and Negami to

a distribution of relaxation times [32]. The frequency representation for the complex modulus as found by the empirical Havriliak-Negami model function as [33]

$$M^*(\omega) = M_\infty + \frac{M_0 - M_\infty}{\left[1 + (j\omega\tau_{HN})^\alpha\right]^\beta} \qquad (4)$$

where M_∞ and M_0 are the unrelaxed and relaxed moduli, ω is the excitation frequency and τ_{HN} is the average relaxation time. The parameter α $(0 < \alpha < 1)$ broadens the width of the relaxation as it decreases in value; the parameter β $(0 < \beta < 1)$ causes a skewing or asymmetry in the modulus in both real and imaginary parts as a function of frequency.

Table 2 gathers the parameters obtained for the fitting of the loss peaks observed in Figures 8, 9, 10 and 11, for *M"(w)* spectra, by means of the HN equation (4). The skewed form of the curves proceeds from ion-ion interactions and the high values of the β_{HN} parameter suggest the absence of those interactions as a consequence of the combined effect of the relatively low concentration of ionic species in those materials and the rigidity of the polymeric matrix that hinders ion-ion interactions. Actually, a second parameter that is in good agreement with this reasoning can be obtained from the full width at half maximum of the *M"* peak in Figures 8-11. The values of this parameter for **KN7**, **KN8**, **KN9** and **KN10** are 1.3, 1.4, 1.2 and 1.2, respectively, which are higher than the one corresponding to a single Debye peak (1.144). This suggests that the conductive peak includes not only pure ionic contributions but also electrodes polarization effects. It has been proven before that ion-ion interaction contributes to the width of the loss peak [34].

In Figure 12 we plot the isothermal loss modulus peaks curves and their fit according to the Havriliak-Negami equation (4) for three temperatures, 238, 268 and 298 K, for the SILLPs **KN7**, **KN8**, **KN9** and **KN10**, respectively. The agreement between the experimental data and the fitting curves (solid lines) is very good. From the values shows in table 2 we can observe that α and β values from both frequency and time domains, for all the SILLPs, are not dependent on temperature. A similar behavior has been reported by Alvarez et al. for poly(hydroxyl ether of bisphenol-A) polymers [35].

The f_M is the frequency at which *M"(f)* reach the maximum value and $\tau_{max}=1/2\pi f_M$. The double-logarithmic plot of figure 13 show the dependence of the

conductivity with $\omega_{max\ (M'')} = 1/\tau_{max}$ (i.e. $f_M = 1/2\pi\tau_{max(M'')}$ characteristic relaxation times of the modulus and ω_c characteristic frequency where the Impedance of the SILLPs reach a plateau which directly yields the dc-conductivity, σ_0, (σ' diagram), (i.e. $f_c = 1/2\pi\tau_c$) is presented for **KN7**, **KN8**, **KN9** and **KN10** plot. In the imaginary part of the modulus spectra, a relaxation peak is observed for all the SILLPs for the conductivity processes of different intensity. The intensity of the modulus relaxation peak is 0,16, 0,23, 0,22 and 0,15 for **KN7**, **KN8**, **KN9** and **KN10**, respectively; whereas no peak is observed in the dielectric spectra, see Figure 7, for **KN10**.

4. Discussion

The ionic conductivity of **KN9** and **KN10** is nearly two orders of magnitude higher than that of **KN7** and **KN8**, respectively, whatever temperature as a basis of comparison is taken. In principle, one could think that electrical transport in the materials is carried out by the mobile anions. In this case, the results suggest that the mobility of NTf_2^- is higher than that of Cl^-, a result opposite to what one at first sight would expect if the anions volume were determinant in the conductive process. However, strong Coulombic forces between cations and anions in absence of humidity, makes this transport mechanism unlikely. Moreover, charge transport by anions would be dependent on frequency. Therefore to explain the conductivity of these materials it is necessary to postulate charge delocalization between cations and anions as mainly responsible for the conductivity independent of frequency that **KN7**, **KN8**, **KN9** and **KN10** exhibit. Owing to the high electronegativity of the chloride anion, charge delocalization is obviously easier for NTf_2^- than for Cl^- and hence the higher conductivity of **KN9** and **KN10**. Similar behavior and results have been found for other supported ionic liquid-like phases prepared by anchoring imidazolium moieties onto highly crosslinked poly(p-chloromethylstyrene-codivinylbenzene) monolithic matrices [12]. In the case of linear polymerized ionic liquids, dielectric relaxation studies have suggested that the transport mechanism is achieved by the formation and dissociation of ion-pairs formed between a positively charged imidazolium subunit in the polymer and the anion [36]. It is noteworthy that although the order of magnitude is similar, a small increase in the conductivity is observed for the systems having a methyl substituent at C2. This is

particularly significant when the conductivity values of **KN8** are compared with those previously reported for **KN5** (i.e. an almost threefold increase is calculated at 388 K) [11]. This seems to indicate that the interaction C2-H←X^- is a contributing factor in this regard. For T > Tg, an increase in temperature increases the mobility of the chains, facilitating charge delocalization between neighboring cations and anions.

The Barton-Nakajima-Namikawa (BNN) relation [37-39], has been shown to be a direct result of a combination of Einstein-Smoluchowski, and Maxwell relations. On the basis of the quantitative agreement between f_c and the structural α-relaxation rate as measured by dynamic mechanical spectroscopy, it is been concluded that glassy dynamics enhance charge transport in ionic liquids [40]. Krause et al. in ref. 41 studying the charge transport and dipolar relaxations in imidazolium based ionic liquids has been shown that the dielectric spectra are described at higher frequencies in terns of dipolar relaxations whereas hopping conduction in a random spatially varying energy landscape is quantitatively the spectra dominate at low frequencies, exhibing the dielectric strength a strong dependence on the anion. Similar conclusions we can do in our study, where we are observed higher conductivity when the samples containing NTf^{-2} than Cl^- ions and with addition of methyl group. In this regard, it must be taken into consideration that solution studies have highlighted the high importance that both the nature of the counteranion and the lenght of the alkyl N-substitution can have, for instance, on the melting points of ILs. Thus, for instance, substituting a methyl group by a butyl group in N-alkyl, N'-methyl imidazolium chloride is accompanied by a decrease in the melting point of ca. 60ºC. On the other hand, substitution of the anion from chloride to bistriflamide in the N-butyl, N'-methyl imidazolium is reflected in a decrease of the melting point of ca. 130ºC [42,43]. This highlights that, as observed in the case of SILLPs, the counteranion has a more pronounced effect than changes in the nature of the alkyl substituent (R1 in chart 1).

Similar results have been reported by Fu et al. in Ref. 44 for PPG-$LiCF_3SO_3$ system with higher salt concentration. Therefore, the conduction in polymer electrolytes takes place through charge migration of ions between coordinated sites of the polymer along with its segmental relaxation. The lack of ion-ion interactions is also made evident in the fact that the conductivities of **KN7**, **KN8**, **KN9** and **KN10** are a thermally activated process. At high frequencies, the secondary absorptions arising from local motions of moieties involving the imidazolium group, which presumably arise from

rotations about the C^{ar}-CH_2-N bonds of the ILs moieties, are affected by the nature of the counterion.

5. Conclusions

The conductivity of the SILLP systems obeys the universal power law as described by Jonscher [16]. The SILLPs with the NTf_2^- anion present a conductivity being nearly two orders of magnitude above that of the system with Cl^- as counterion.

The modulus formalism is an appropriate representation of dielectric data for analysis of ionic conductivity relaxations when the dielectric permittivity ε" is high increasing with the temperature in the low frequency region due to conduction process such as has been observed in our SILLPs.

The high values of the β parameter suggests the absence of ion-ion interactions as a consequence of the combined effect of the relatively low concentration of ionic species in these materials and the rigidity of the polymeric matrix that hinder ion-ion interactions. The difference of the conductive results between Cl^- and NTf_2^- can be related with the energy of ion-ion dissociation. Regarding the structural changes in the structure of the imidazolium cations, it can be seen that the substitution at the C2 position of the imidazolium ring has some effects on the conductivity of these SILLPs. This is clearly illustrated when comparing the conductivities observed for **KN8** (with a methyl substituent at C2) with the related **KN5** (lacking the methyl group at C2) formerly studied [11]. The overall data indicate that hydrogen bonding plays a role in terms of intermolecular interactions for imidazolium subunits in SILLPs. A similar trend is observed when the SILLPs containing NTf_2^- instead of Cl^- as the anion are compared. In the same way, the change of the N-methyl substituent by a more hydrophobic butyl fragment has also a minor influence in the conductivity of the resulting SILLPs as can be seen, for instance, from the comparison of the results with previously studied systems differing just in this structural feature [11]. Thus, for this kind of SILLPs, characterized by a high degree of crosslinking and a low degree of functionalization, it is the nature of the counter anion the main structural parameter affecting the observed conductivity. Additional studies are being carried out in order to fully understand the role played by other parameters such as the monomeric composition of the matrix or the loading of

imidazolium subunits, not only on the values of conductivity observed but also on the mechanisms involved in the conduction process.

Acknowledgments

Then authors are grateful to Dr. Abel Gacía-Bernabé for assistance with the experiments. This work was supported by the Instituto de la Pequeña y Mediana Industria Valenciana (IMPIVA), Grant IMIDIC 2009/155. We thank the Spanish Ministerio de Ciencia y Tecnología (CTQ2008-04412/BQU and CTQ2008-04309/BQU) and Bancaixa-UJI (P1 1A2009-58) for financial support.

References

[1] P. Wasserscheid, T. Welton, *Ionic Liquids in Synthesis*; Wiley-VCH: Weinheim, Germany, **2007.**[2] N. V. Plechkova, K. R. Seddon, *Chem. Soc. Rev.*, 2008, **37**, 123.

[3] a) M. Moniruzzaman, N. Kamiya, M. Goto, *Org. Biomol. Chem.*, 2010, **8**, 2887; b) L. Ding, T. He, Y. Xiong, J. Wu, L. Chen, G. Chen, *Prog. Chem*., 2010, **22**, 298; c) Y. Yoshida, G., Saito, *Phys. Chem. Chem. Phys*., 2010, **12**, 1675; d) D. MacFarlane, M. Forsyth, *The Handbook of Ionic Liquids*, *Electrochemistry*, Wiley-VCH: Weinheim, Germany, **2008**.

[4] H. Olivier-Bourbigou, L. Magna, D. Morvan, *Applied Catal. A: General*, 2010, **373**, 1.

[5] M. Armand, F. Endres, D. R. MacFarlane, H. Ohno, B. Scrosati, *Nat. Mater*., 2009, **8**, 621.

[6] R. Kawano, T. Katakabe, H. Shimosawa, Md. K. Nazeeruddin, M. Grätzel, H. Matsui, T. Kitamura, N. Tanabe, M. Watanabe, *Phys. Chem. Chem. Phys*., 2010, **12**, 1916.

[7] R. Giernoth, *Angew. Chem. Int. Ed*., 2010, **49**, 2834.

[8] a) L. Ford, J.R. Harjani, F. Atefi, M. T. Garcia, R. D. Singer, P. J. Scammells, *Green Chem*., 2010, **10**, 1783; b) T.P. Thuy Pham, C.-W. Cho, Y.-S., Yun, *Water Research*, 2010, **44** ,352.

[9] a) C. P. Mehnert, *Chem. Eur. J.*, 2004, **11**, 50; b) A. Riisager, R. Fehrmann, S. Flicker, R. van Hal, M. Haumann, P. Wasserscheid, Angew. Chem. Int. Ed., 2005,

44, 815; c) Y. Gu, G. Li, *Adv. Synth. Catal.*, 2009, **351**, 817, d) C. Van Doorslaer, J. Wahlen, P. Mertens, K. Binnemans, D. De Vos, *Dalton Trans*., 2010, **39**, 8377.

[10] O. Green , S. Grubjesic, S. Lee, M. A. Firestone, *Polym. Rev*., 2009,**49**, 339.

[11] A. Garcia-Bernabé, V. Compañ, M. I. Burguete, E. Garcıa-Verdugo, N. Karbass, S. V. Luis, E. Riande, *J. Phys. Chem. C*, 2010, **114**, 7030.

[12] V. Sans, N. Karbass, M. I. Burguete, V. Compañ, E. García-Verdugo, S. V. Luis, M. Pawlak, *Chem. Eur. J*., 2011, **17**, 1894.

[13] a) N. Karbass, V. Sans, E. García-Verdugo, M. I. Burguete, S. V. Luis, *Chem. Commun.*, 2006, 3095; b) P. Lozano, E. García-Verdugo, R. Piamtongkam, N. Karbass, T. DeDiego, M. I. Burguete, S. V. Luis, J. L. Iborra, *Adv. Synth. Catal.*, 2007, **349**, 1077; c) M. I. Burguete, H. Erythropel, E. Garcia-Verdugo, S. V. Luis, V. Sans, *Green Chem.*, 2008, **10**, 401.

[14] E. Barsoukov, J.R. MacDonald, *Impedance Spectroscopy. Theory, Experiment, and applications.* Second Edition., Chapter 2, pp. 87-88. Wiley-Interscience, **2005.**

[15] W.W. Bode, *Network Analysis and Feedback Amplifier Design*, Van Nostrand, Princenton, N.J., **1956**.

[16] A. K. Jonscher, *Nature*, 1977, **267**, 673.

[17] N.G. McCrum, B.E. Read and G. Williams, *Anelastic and Dielectric Effect in Polymeric Solids*, Dover Publications, New York, **1991**.

[18] C. T. Moynihan, *J. Non-Cryst. Sol.*, 1994, **172-174**, 1395; *ibid* 1996, **203**, 359.

[19] C. T. Moynihan, *Solid State Ionics*, 1998, **105**, 175.

[20] S. R. Elliot, *J. Non-Cryst. Sol.,* 1994, **170**, 97.

[21] B. Roling, *Solid State Ionics*, 1998, **105**, 185.

[22] I. M. Hodege, K. L. Ngai, C. T. Moynihan, *J. Non-Cryst. Solids*, 2005, **351**, 104.

[23] K. L. Ngai, C. León, *Solid State Ionics*, 1999, **125**, 81.

[24] F. S. Howell, R. A. Bose, P. B. Macedo, C. T. Moynihan, *J. Phys. Chem.*, **1974**, *78*, 639.

[25] C. T. Moynihan, *J. Phys. Chem.*, **1966**, *70*, 3399.

[26] C. T. Moynihan, N. Balitact, L. Boone, T. A. Litovitz, *J. Chem. Phys.*, **1971**, *55*, 3013.

[27] Kremer, F.; Schönhals, A. *Broadband Dielectric Spectroscopy*; Springer: Berlin, 2003).

[28] Dyre, J.C., *J. Phys. C: Solid State Phys.*, **1986**, 19, 5655.

[29] Krause, C.; Sangoro, J.R.; Iacob, C.; Kremer, F., *J. Phys. Chem. B,* **2010**, *114*, 382.

[30] J. S. Kim, *J. Phys. Soc. Jpn.*, **2001**, *70*, 3129.

[31] J. Liu, C.-G. Duan, W.-G. Yin, W. N. Mei, R. W. Smith, J. R. Hardy, *J. Chem. Phys.*, **2003**, *119*, 2812.

[32] S. Havriliak, S. Negami, *Polymer*, **1967**, *8*, 161.

[33] E. Neagu, P. Pissis, L;Apekis, J. L. Gomez-Ribelles, *J. Phys. D: Appl. Phys.*, **1997**, *30*, 1551.

[34] K. L. Ngai, J. Habasaki, Y. Hiwatari, C. Leon. *J. Phys.: Condens. Matter.*, **2003**, *15*, S1607.

[35] F. Alvarez, A. Alegría, J. Colmenero, *Physical Review B*, **1991**, ***44***, 7306.

[36] K. Nakamura, T. Saiwaki, K. Fukao, *Macromolecules*, 2010, **43**, 6092.

[37] J. L. Barton, L. Verres, *Refract*. **1966**, *20*, 328

[38] T. Nakajima, Annual Report, Conference on Electric Insulation and Dielectric Phenomena; National Academy of Sciences: Washington DC, 1971.

[39] H. Namikawa, *J. Non-Cryst. Solids*, **1975**, *18*, 173.

[40] J. R. Sangoro, C. Iacob, A. Serghei, C. Friedrich, F. Kremer, *Phys. Chem. Chem. Phys.*, **2009**, *11*, 913.

[41] C. Krause J. R. Sangoro, C. Iacob, F. Kremer, *J. Phys. Chem. B,* **2010**, *114*, 382.

[42] C. P.Fredlake, J. M. Crosthwaite, D.G. Hert, S. N. V. K. Aki, J. F. Brennecke, *J. Chem. Eng.*, **2004**, *49*, 954.

[43] J. G. Hudleston, A. E. Visser, W. M. Reichert, H. D. Willauer, G. A. Broker, R. D. Rogers, *Green Chem.*, **2001**, *3*, 156.

[44] Y. Fu, K., Pathmanathan, J. R. Stevens, *J. Chem. Phys.*, **1991**, *94*, 6323.

Legend of Figures

Figure 1. Scheme showing the synthesis of SILLPs. i) 30% (w/w) of a mixture 1:2 (40:60 by weight) in a porogen mixture (75:25 dodecanol:toluene by weight) 1% AIBN, 70^{o}C, 24 h. ii) 80^{o}C. iii) $LiNTf_2$, acetone:water (1:1). iii) $LiNTf_2$ in MeOH/water, RT.

Figure 2. DSC curves for **KN7** (square), **KN8** (circle), **KN9** (up triangle) and **KN10** (down triangle): second run. The magnifications show the transition temperature more clearly visible.

Figure 3. a) Bode diagrams for **KN7** showing the logarithm of the magnitude of the impedance and the phase angle at several temperatures: (square) 398K, (circle) 388K, (up triangle) 378K, (down triangle) 368K, (diamond) 358K, (left triangle) 348K, (right triangle) 338K, (hexagon) 328K, (star) 318K, (pentagon) 308K and (plus) 298K. Solid symbols for impedance and open symbols for phase angle; b) real part of the conductivity versus frequency for the same systems; c) imaginary part of the conductivity versus frequency for the same systems.

Figure 4. Bode diagrams for **KN9** showing the logarithm of the magnitude of the impedance and the phase angle at several temperatures: (square) 398K, (circle) 388K, (up triangle) 378K, (down triangle) 368K, (diamond) 358K, (left triangle) 348K, (right triangle) 338K, (hexagon) 328K, (star) 318K, (pentagon) 308K and (plus) 298K. Solid symbols for impedance and open symbols for phase angle; b) real part of the conductivity versus frequency for the same systems; c) imaginary part of the conductivity versus frequency for the same systems.

Figure 5. Activation plot for different characteristic electrical rates ω_c (as obtained from Bode diagram) and $\omega_{max\ (M")}$ (as obtained from the maximum of M"(ω)) for **KN7** (squares), **KN8** (circles), **KN9** (triangles up) and **KN10** (triangles down) SILLPs, respectively.

Figure 6. Activation plot for the dc-conductivity σ_0, obtained from Bode diagram for **KN7** (triangles down), **KN8** (triangles up), **KN9** (squares) and **KN10** (circles) SILLPs, respectively.

Figure 7. Real (top) and loss (bottom) components of the complex dielectric permittivity for **KN10** at several temperatures: (square) 398K, (circle) 388K, (up triangle) 378K, (down triangle) 368K, (diamond) 358K, (left triangle) 348K, (right triangle) 338K, (hexagon) 328K, (star) 318K, (pentagon) 308K and (plus) 298K.

Figure 8. Components of the complex dielectric modulus in the frequency domain for **KN7** at several temperatures: (square) 398K, (circle) 388K, (up triangle) 378K, (down triangle) 368K, (diamond) 358K, (left triangle) 348K, (right triangle) 338K, (hexagon) 328K; open symbols for real dielectric modulus component and solid symbols for loss dielectric modulus component.

Figure 9. Components of the complex dielectric modulus in the frequency domain for **KN8** at several temperatures: (square) 398K, (circle) 388K, (up triangle) 378K, (down triangle) 368K, (diamond) 358K, (left triangle) 348K, (right triangle) 338K, (hexagon) 328K; open symbols for real dielectric modulus component and solid symbols for loss dielectric modulus component.

Figure 10. Components of the complex dielectric modulus in the frequency domain for **KN9** at several temperatures: (square) 398K, (circle) 388K, (up triangle) 378K, (down triangle) 368K, (diamond) 358K, (left triangle) 348K, (right triangle) 338K, (hexagon) 328K, (star) 318K; open symbols for real dielectric modulus component and solid symbols for loss dielectric modulus component. Inset: Magnification for the high frequencies region.

Figure 11. Components of the complex dielectric modulus in the frequency domain for **KN10** at several temperatures: (square) 398K, (circle) 388K, (up triangle) 378K, (down triangle) 368K, (diamond) 358K, (left triangle) 348K, (right triangle) 338K, (hexagon) 328K, (star) 318K, (pentagon) 308K; open symbols for real dielectric modulus component and solid symbols for loss dielectric modulus component.

Figure 12. Isothermal loss modulus peaks curves and their fits to the Havriliak-Negami expression at 338K (right triangle), 368K (down triangle) and 398 K (square), respectively. (a) **KN7**, (b) **KN8**, (c) **KN9** and (d) **KN10**.

Figure 13. Double logarithmic plot of the dc-conductivity σ_0, versus the characteristic rates of charge transport obtained from real part of the conductivity diagrams (σ') ω_c (solid symbols) and from the maximum of M"(ω), $\omega_{max\ (M")}$ (open symbols) for **KN7** (squares), **KN8** (circles)**, KN9** (up triangle) and **KN10** (diamond) SILLPs, respectively.

FIGURES

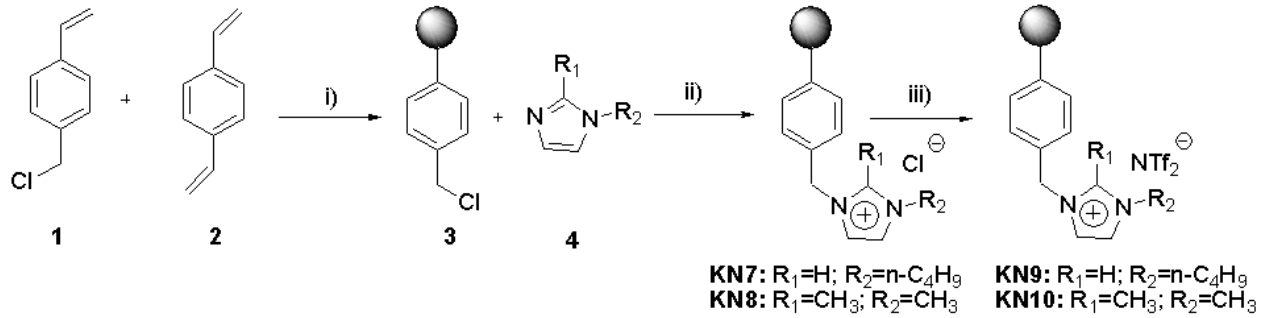

Figure 1.

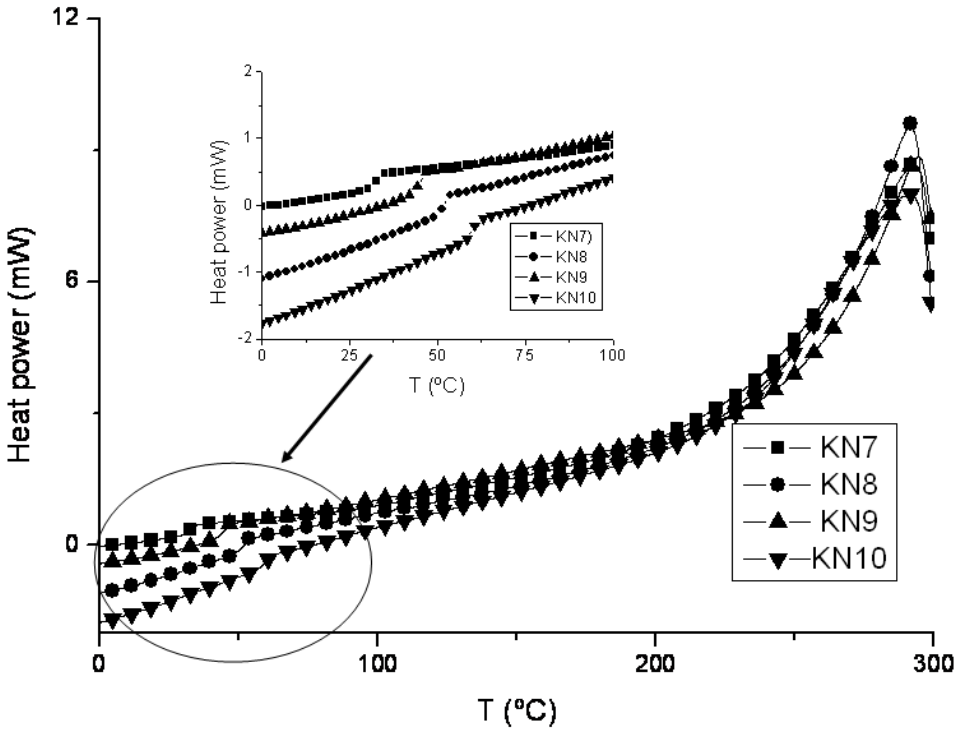
Heat power (mW)
T (ºC)
KN7
KN8
KN9
KN10
Heat power (mW)
T (ºC)
KN7)
KN8
KN9
KN10

Figure 2.

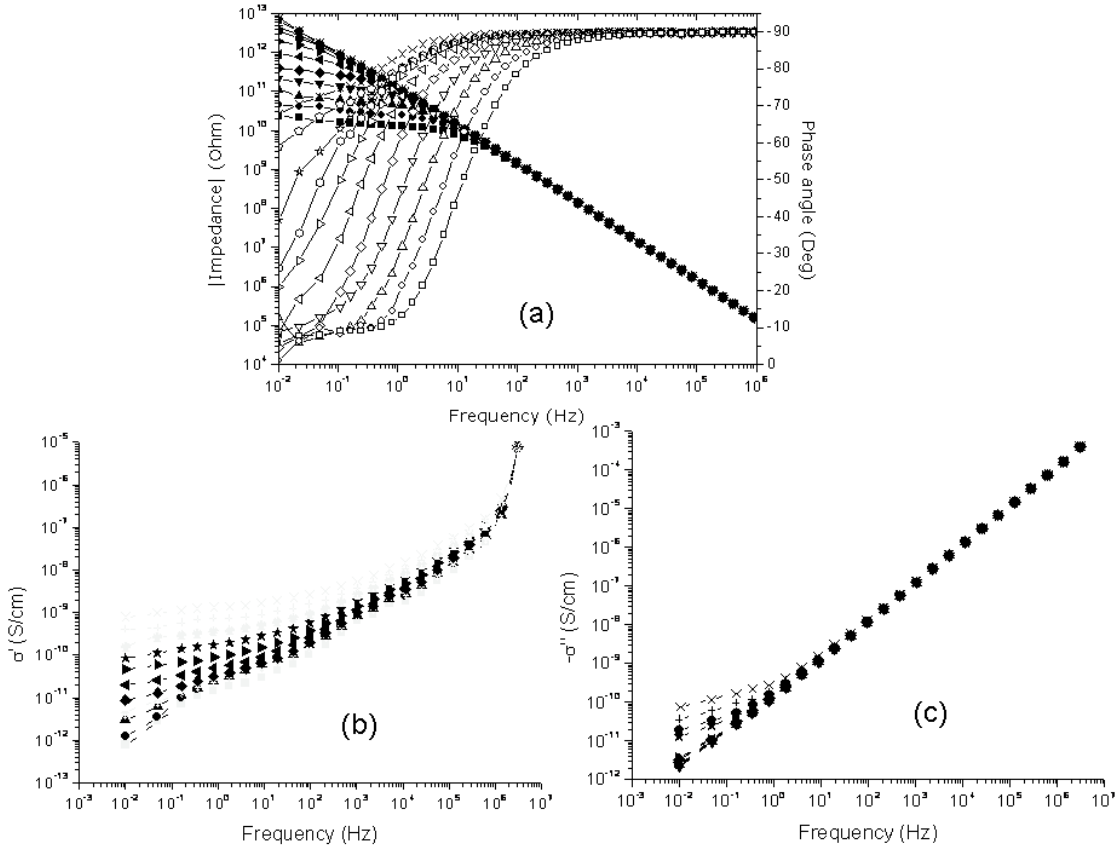
|Impedance| (Ohm)
Phase angle (Deg)
Frequency (Hz)
(a)
σ' (S/cm)
Frequency (Hz)
(b)
-σ'' (S/cm)
Frequency (Hz)
(c)

Figure 3.

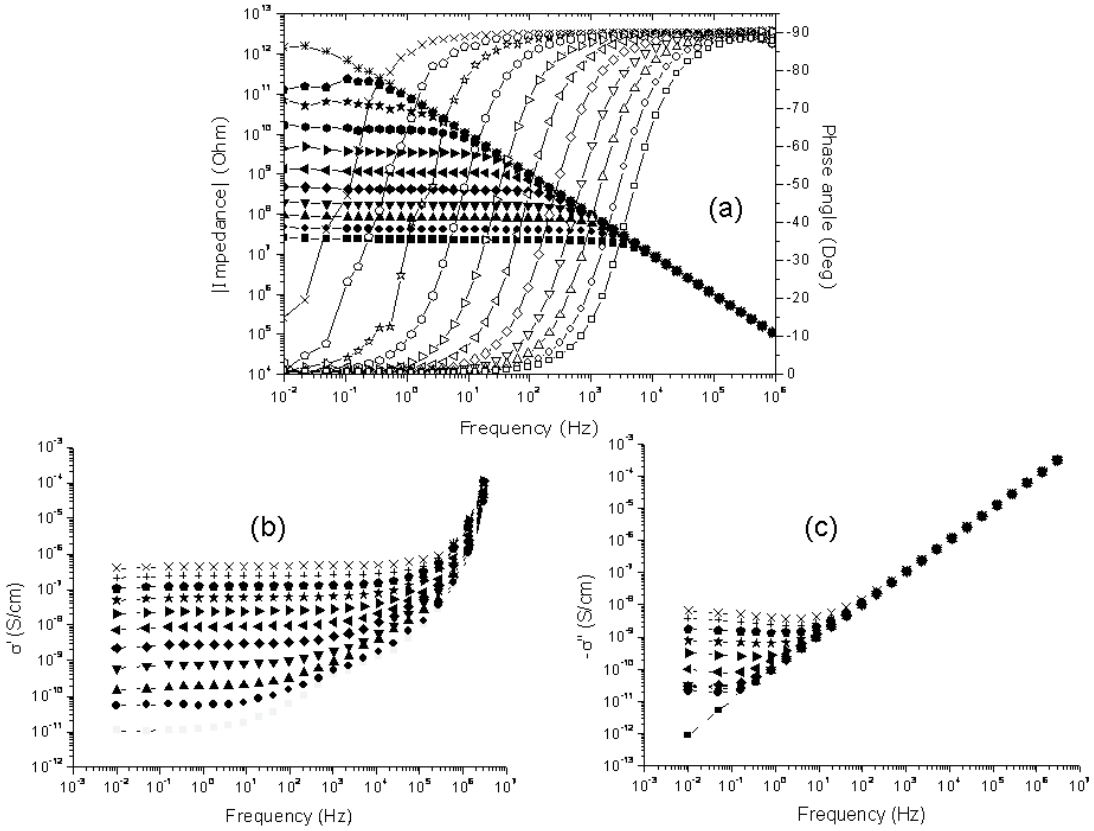

Figure 4.

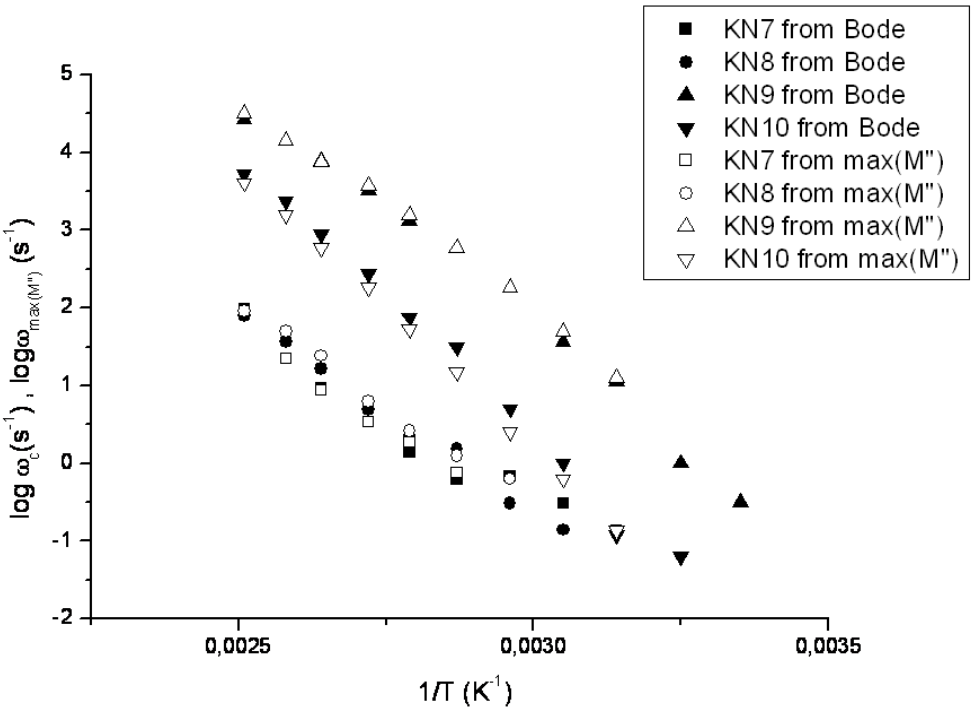

Figure 5.

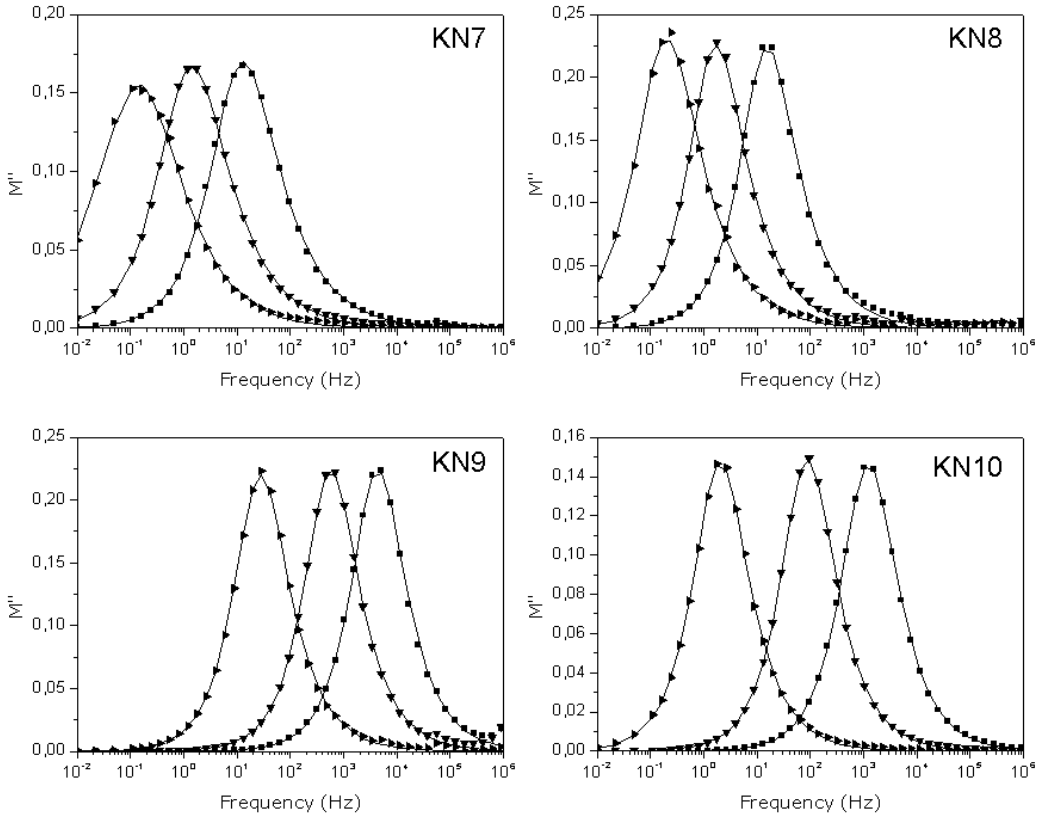

Figure 6.

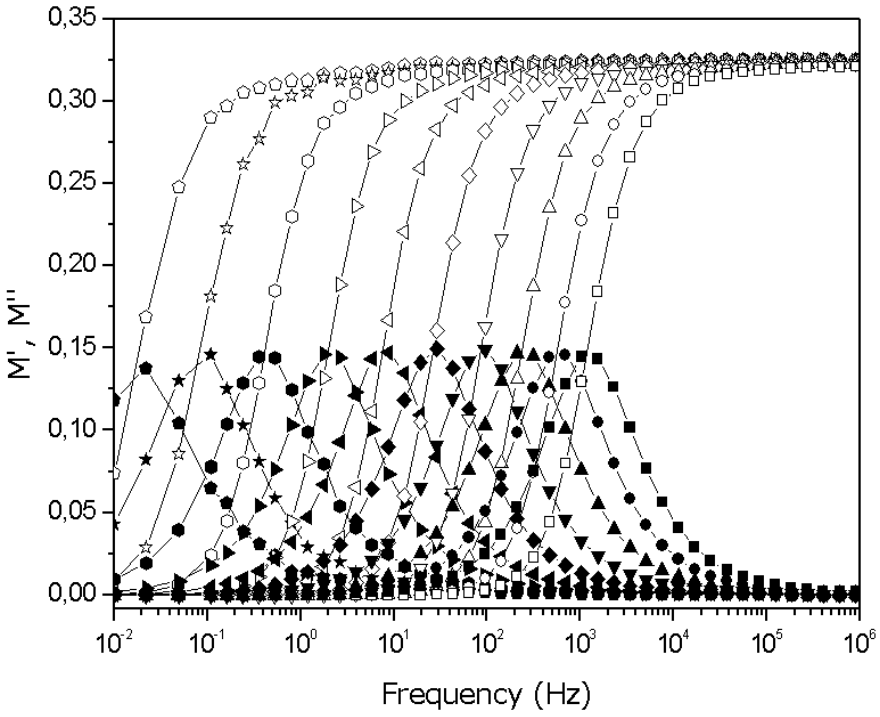

Figure 7

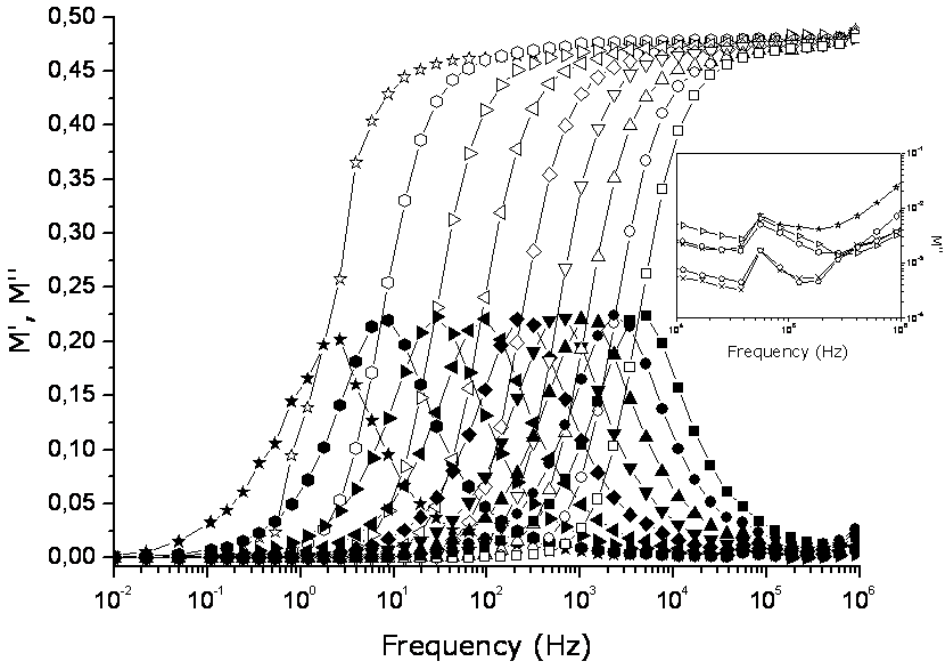

Figure 8.

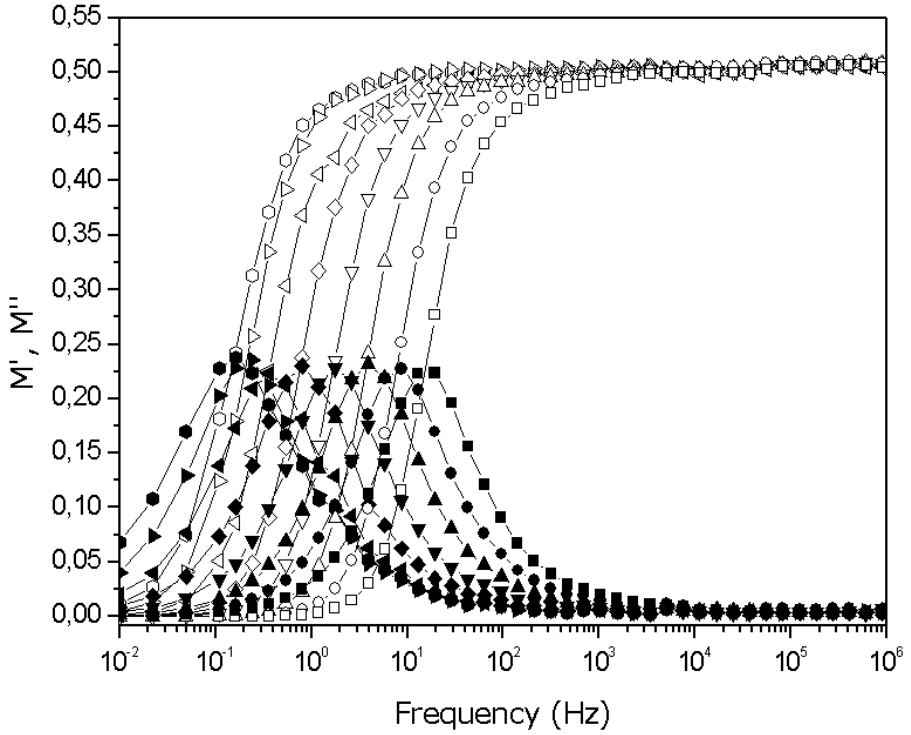

Figure 9.

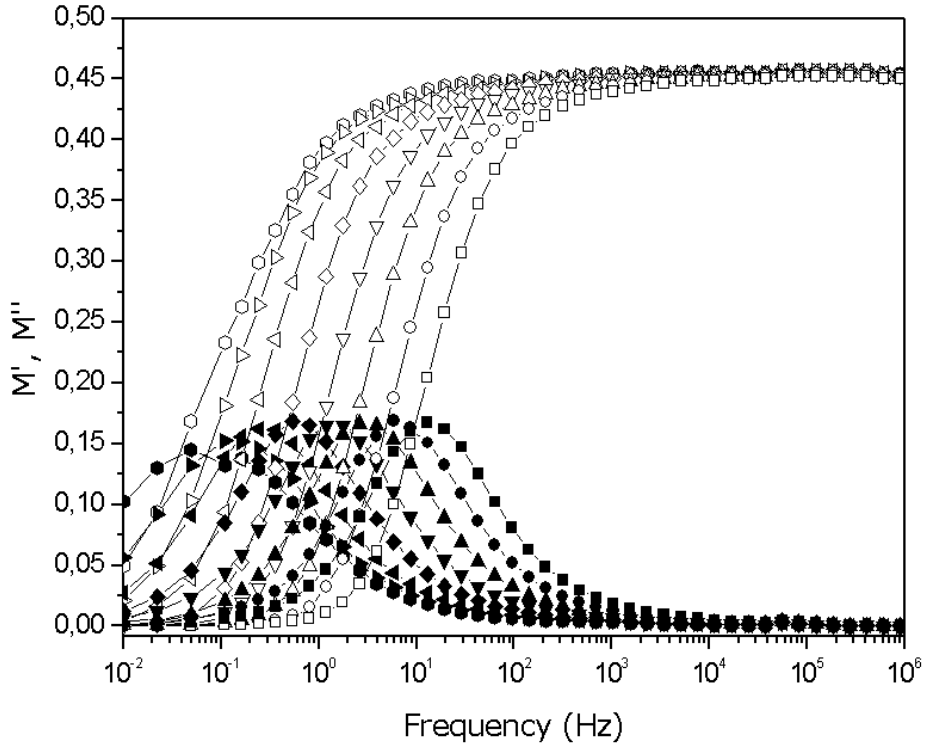

Figure 10.

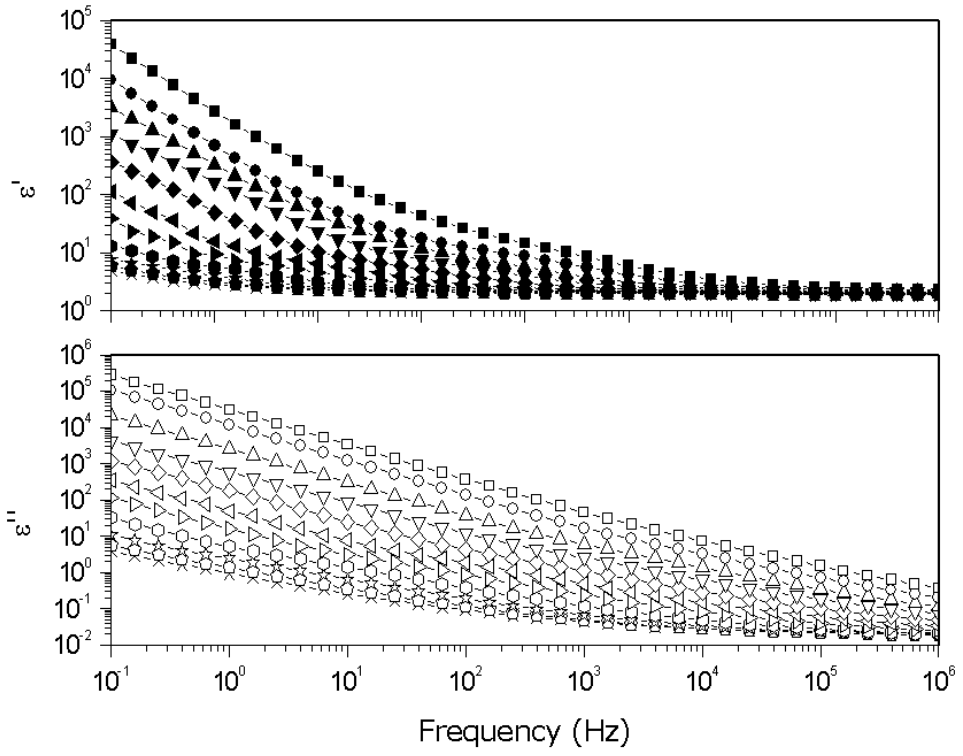

Figure 11.

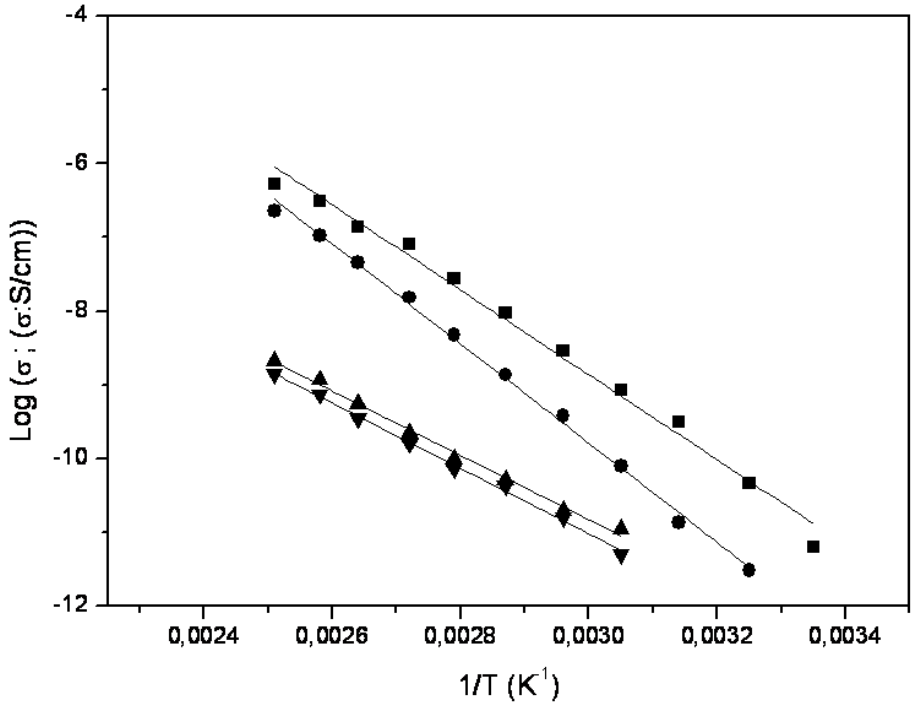

Figure 12.

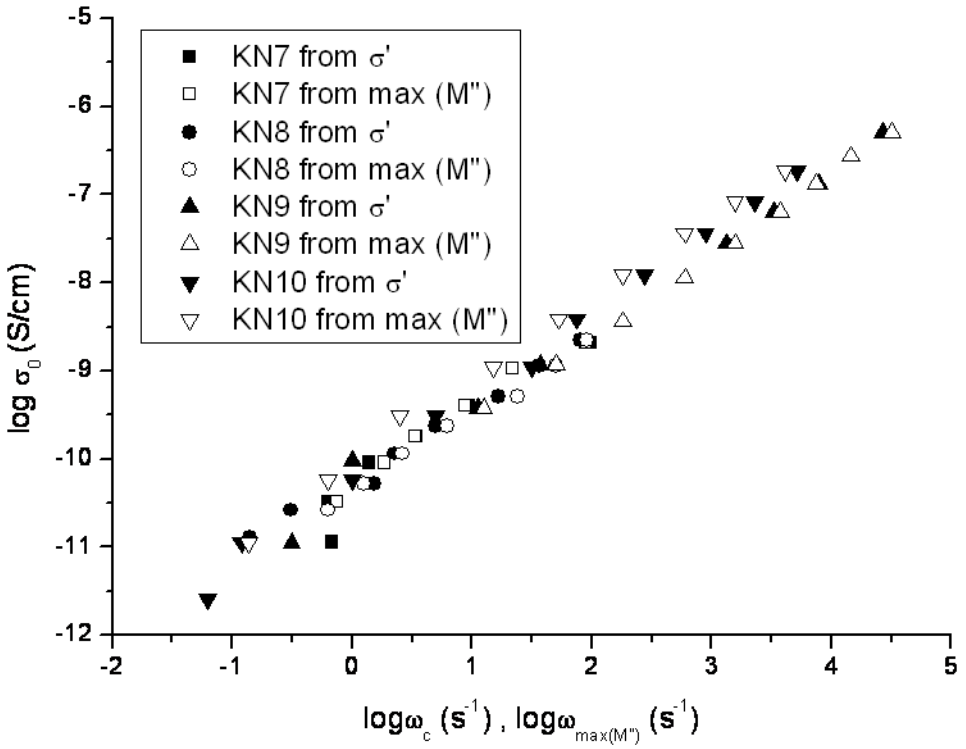

Figure 13.